Structural, thermal, rheological and mechanical properties of polypropylene/graphene nanoplatelets composites: effect of particle size and melt mixing conditions

Quentin Beuguel, Alice Mija, Bruno Vergnes, Edith Peuvrel-Disdier

Structural, thermal, rheological and mechanical properties of polypropylene/graphene nanoplatelets composites: effect of particle size and melt mixing conditions

Journal:	*Polymer Engineering & Science*
Manuscript ID	PES-17-0528.R1
Wiley - Manuscript type:	Research Article
Date Submitted by the Author:	n/a
Complete List of Authors:	BEUGUEL, Quentin; Mines ParisTech, CEMEF, UMR CNRS 7635 MIJA, Alice; Universite de Nice Sophia Antipolis, ICN – UMR CNRS 7272 Vergnes, Bruno; Mines ParisTech, CEMEF, UMR CNRS 7635 PEUVREL-DISDIER, Edith; Mines ParisTech, CEMEF, UMR CNRS 7635
Keywords:	polyolefins, nanoparticles, nanocomposites, morphology, rheology

Structural, thermal, rheological and mechanical properties of polypropylene/graphene nanoplatelets composites: effect of particle size and melt mixing conditions

Quentin Beuguel[1], Alice Mija[2], Bruno Vergnes[1], Edith Peuvrel-Disdier[1]

[1] MINES ParisTech, PSL Research University, CEMEF - Centre de Mise en Forme des Matériaux, UMR CNRS 7635, CS 10207, 06904 Sophia-Antipolis, France

[2] Université de Nice Sophia-Antipolis, ICN – UMR CNRS 7272, Parc Valrose, 06108 Nice Cedex 2, France

Correspondence to: E. Peuvrel-Disdier (E-mail: edith.disdier@mines-paristech.fr)

ABSTRACT

Graphene nanoplatelets (GNP) of various sizes were mixed with polypropylene (PP) in an internal mixer to prepare composites. The effects of mixing conditions, GNP size and concentration in composites were investigated. The composites were characterized at different scales, using electron microscopy, X-ray diffraction, thermogravimetric analysis, and rheometry. It was shown that the PP/GNP composites had to be considered as non-intercalated and non-exfoliated microcomposites. However, the thermal, rheological and mechanical properties of the PP/GNP microcomposites were improved with respect to that of the matrix and similar to those of thermoplastic/organoclay or reduced graphene nanocomposites. In the best cases, storage modulus plateau in the glassy domain was increased by 30% and onset of degradation temperature by 40°C. Finally, in the investigated range of this study, the mixing conditions applied in the internal mixer did not affect the structural and rheological properties of the PP/GNP composites.

KEYWORDS: Polyolefins; Nanoparticles; Nanocomposites; Morphology; Rheology

INTRODUCTION

Nonpolar polypropylene (PP) is largely used for its low cost and its easy processability. For several decades, attention has been paid to improve PP properties by adding nanofillers. Montmorillonite was largely used for its availability, the shape anisometry of its nanoplatelets and its exfoliation ability after organo-modification [1]. Besides, polymer/carbon nanotube (CNT) composites were developed because of the high aspect ratio, mechanical, thermal and electrical properties of CNT [2, 3]. Since 2004 and the isolation of single graphene sheets from graphite by micromechanical cleavage [4], the enthusiasm for this new nanofiller has increased. Graphene combines both layered silicate and carbon nanotube characteristics [5, 6]. However, graphene preparation is still restrictive and expensive. Two main promising ways are being explored in order to obtain graphene sheets in large quantities from graphite [6, 7]. The first method consists in obtaining either chemically [8] or thermally [9, 10] reduced exfoliated graphene from graphite oxide [11]. However, the physical properties of reduced graphene, especially its electrical properties, are damaged by oxidation traces [8–10]. Another method has therefore been developed. It consists in a graphite acid intercalation followed by a strong thermal shock and ultrasonication of the expanded graphite suspension [12]. The ultrasonication of the expanded graphite suspensions results in stacks of several tens of nanometers in thickness [12, 13]. Recently Zhao et al. [14] developed a mechanical delamination process followed by centrifugation of these particles in order to get graphene nanoplatelets (GNP) with a thickness of a few nanometers.

Polymer/graphene nanocomposites can be elaborated by solution mixing [15-17], in situ polymerization [18-19] or melt mixing using different techniques: three-roll mill [20], internal mixer [21], micro-compounder [22, 23], and twin-screw extruder [17, 24]. The reduced graphene can be functionalized to favour affinity with the matrix [25, 26], or not [27]. The objective is to improve the mechanical, thermal, electrical or gas barrier properties of the matrix. However, obtaining a nanodispersion of untreated GNP in a non-polar matrix by melt mixing remains a challenge [28-30]. Nevertheless, even though solvent dispersion appears more efficient than melt mixing [17], the latter is the only technique that can be used at

an industrial scale without environmental issues. Recently, authors proposed cryogenic impact milling [31] or ultrasound-assisted extrusion [32] to enhance the exfoliation of PP/GNP composites.

The aim of the present study was to assess the potential of three grades of GNP, differing in their preparation processing and resulting sizes, on PP/GNP composites properties. Composites were elaborated by melt mixing in an internal mixer. The effect of GNP size and concentration on the structural, rheological, thermal and mechanical properties of composites was investigated. A close attention was paid to the influence of mixing conditions on the structural and rheological properties of these composites.

MATERIALS AND METHODS

Materials

Composites were prepared from commercial isotactic polypropylene (PP) matrix (referred as Moplen HP400R) supplied by LyondellBasell. The PP density was 0.9, the number and weight average molecular weights were, respectively, 59 $kg.mol^{-1}$ and 205 $kg.mol^{-1}$. The Newtonian viscosity was close to 1,460 Pa.s at 180°C.

GNP were provided by Knano (Xianen, China) under references KNG-180, KNG-150 and KNG-G5. KNG-180 and KNG-150 grades were obtained from graphite through a three-step thermochemical process: i) graphite was first intercalated by sulfuric acid under stirring, washed and dried, ii) it then underwent a thermal shock and iii) expanded graphite was finally ultrasonicated in a hydroalcoholic solution. From this step, particles are considered as GNP [12]. These two GNP essentially differ in size (Table 1). The application of an additional ball milling process in a good solvent, followed by centrifugation, was applied to KNG-180. The resulting GNP is referred to as KNG-G5 [14]. Figure 1 shows the different GNP powders. Supplier data on GNP characteristics are reported in Table 1. The KNG-180 presents large and thick tactoids, the size of which is largely reduced in KNG-150. KNG-G5 is even thinner, with a thickness of about a dozen layers of graphite.

Methods

All composites were elaborated by melt mixing at T = 180°C using an internal mixer (Haake Rheomix 600), in three steps: i) PP was introduced and melted for 2 min at the rotor speed of N = 20 rpm; ii) GNP were introduced for 8 min at the same rotor speed (N = 20 rpm) (this duration was required because the introduction of GNP was tricky, due to their low bulk density); iii) both PP and GNP were mixed (dispersion phase) for 6 min at the rotor speed of N = 100 rpm. In this last phase, a mixing time of 12 min and a rotor speed of 200 rpm were also tested to evaluate the influence of processing conditions. After mixing, composites were cooled down under air to room temperature, and compression molded in disk shape with a diameter of 25 mm and a thickness of 1.5 mm, at 180°C for 10 min using a hydraulic press. Composites were prepared with various GNP volume fractions (ϕ_{vol}) ranging from 0.3 to 2%.

Microscale observations on polished samples were carried out using a Scanning Electron Microscope (SEM) (Philips XL30 ESEM), operating at 15 kV. Particles were flake-like and appeared as elongated objects (cross-section of flakes), regardless of the GNP. The few agglomerates with a thickness above 40 µm were excluded from SEM analysis in order to minimize the weight of these seldom agglomerates. On the other hand, the detection of particles with a thickness lower than 0.4 µm was limited by the SEM resolution. These particles were thus not taken into account. The surface coverage percentage S of GNP microparticles (with a thickness between 0.4 and 40 µm) was determined on SEM micrographs at the same magnification for all samples, using Visilog® software after image binarization. At least, 4 micrographs, corresponding to 50 to 300 microparticles, were analyzed for each sample. A statistical study allowed us to estimate the error on S parameter to be ± 10%.

Submicroscale observations were performed using a Transmission Electron Microscope (TEM) (Jeol JEM 1400), equipped with camera (Olympus MORADA SIS), and operating at 100 kV, available at Centre Commun de Microscopie Appliquée (CCMA), Nice Sophia-Antipolis University. Sample structure was investigated on 100 nm thick ultrathin cuts, prepared using Leica FC6 ultracryomicrotome equipped with a diamond knife at -100°C. The average lateral dimension L, thickness e and aspect ratio p_{MET} ($p_{MET} = L/e$) of

GNP particles were determined from measurements on at least 100 particles per sample. These average values were accurate to ± 10%. The specific particle density d_{sp} (average number of particles per μm^2 divided by the filler weight fraction) was also determined. This quantity is assumed to characterize the exfoliation degree [33].

The GNP structure in the composites was also investigated by X-Ray diffraction (XRD) (PANalytical X'pert Pro MPD) in θ-θ position with Cu Kα radiation of 0.154 nm, generated at 45 kV and 30 mA. Experiments were carried out over a 2θ range from 4° to 30°, using steps of 0.08°.

The GNP effect on PP thermal degradation was investigated on samples with a mass around 10 mg (with a precision weighting scale of 0.1 mg), using Mettler-Toledo 851e ThermoGravimetric Analysis (TGA), available at Nice Sophia-Antipolis University. The tests were performed under air flow of 50 mL/min, from 25°C to 1000°C, at 10°C/min. $T_{10\%}$ and $T_{50\%}$ temperatures, corresponding, respectively, to a mass loss of 10% and 50%, were reported. These measurements were reproducible to ± 10 °C. They allowed us to determine, beside the thermal properties, the exact filler volume fraction ϕ_{vol} for each composite.

Oscillatory shear measurements were performed under nitrogen at 180°C, using a controlled stress rheometer (Anton Paar MCR302), equipped with parallel plate geometry (25 mm diameter). Angular frequency sweep tests were carried out in the linear domain (γ = 0.1%) over a range from 100 to 10^{-2} rad.s^{-1}. A time sweep measurement was also performed in the linear domain at 0.1 rad.s^{-1}, and highlighted a perfect thermal stability of PP matrix. Similar tests carried out on PP/GNP composites showed a low increase of viscoelastic properties as a function of time, attributed to GNP structure built-up in the molten state [34]. In any case, rheological data measured within 30 min were reproducible to ± 5%.

Dynamic Mechanical Thermal Analysis (DMTA) tests were carried out in tension, in the linear domain (γ = 0.1%), using DMA BohlinTriton Technology Tritec 2000, at a frequency of 1 Hz. Measurements were carried out on parallelepiped samples (dimensions 20 x 3 x 1.5 mm). Tests were performed from -30 to 165°C at 2°C/min. Storage modulus E', loss modulus E'' and damping factor $\tan\delta = E''/E'$ were measured. Transition

temperatures T_α et $T_{\alpha'}$, corresponding, respectively, to the main relaxation temperature of the amorphous phase and the relaxation temperature of the amorphous phase constrained by crystal or within crystal [35] or due to prefusion mechanisms [36], were reported. Thermomechanical measurements were accurate to ± 5%.

RESULTS AND DISCUSSION

Structural properties of PP/GNP composites

The figure 2 shows SEM and TEM images of PP/1% GNP composites.

KNG-180 and KNG-G5 particles are platelet-like (Figures 2a, 2c, 2d and 2f) while KNG-150 particles are more disk-like (Figures 2b and 2e). There is a large number of very thin microparticles (thickness lower than 0.4 µm) in the PP/KNG-G5 composite (Figure 2c). In comparison there are fewer microparticles with a thickness between 0.4 and 40 µm (particles considered for the estimation of the surface coverage parameter S) in the PP/KNG-G5 composite (Figure 2c) than in PP/KNG-150 and PP/KNG-180 composites (Figures 2a and 2b), as confirmed by *S* measurements (Table 2). All composites are mainly composed of micrometric particles with a few submicronic ones, as reported by Ferreira et al. [37] in the case of PP/exfoliated graphite composites. From TEM measurements, KNG-180 nanoplatelets are longer than KNG-150 and KNG-G5 ones, as expected from the supplier data. However, the values are lower than those presented in Table 1. KNG-G5 particles are respectively 2 and 4 times thinner than KNG-150 and KNG-180 ones, leading to an aspect ratio p_{MET} of 8, 5 and 10 for KNG-180, KNG-150 and KNG-G5 particles, respectively (Table 2). However, measured thicknesses are much greater than those of Table 1, perhaps due to some agglomeration of the initial tactoids. The higher exfoliation degree of KNG-G5 particles, obtained after KNG-180 delamination, is confirmed by specific particle density d_{sp} values. It was also checked that the *S* parameter increases with the filler volume fraction, in agreement with the higher number of microparticles.

Figure 3 shows wide-angle X-Ray diffractograms of PP/1% GNP composites. In addition to the characteristic peaks of the α PP crystalline phase, a peak at 2θ = 26.5° is observed, characteristic of graphene stack

reflection (002), and corresponding to an interlayer distance of 0.34 nm [17, 24]. For an equivalent volume fraction, the less intense graphene peak in PP/KNG-G5 composites indicates a small number of graphene ordered stacks, as observed by He et al. [32] with ultrasound treatment during extrusion. Moreover, no graphene peak shift is observed after melt mixing. This confirms the absence of PP chain intercalation between graphene layers.

To conclude, even though mechanical delamination followed by centrifugation of GNP was shown to efficiently separate nanoplatelets and to allow to prepare colloidal suspensions in solvents [14], all GNPs mixed with molten PP gave rise to microcomposites. The melt mixing process did not allow neither polymer chain intercalation, nor exfoliation of graphene layers, as already reported by some authors [17, 38].

Thermal, rheological and mechanical properties of PP/GNP composites

Figure 4 presents the mass loss for PP/1% GNP composites. For all samples, thermal degradation of PP matrix starts around 230°C but the addition of GNP tends to delay this degradation, as already reported by Kiziltas et al. [39]. In the presence of GNP, the PP degradation occurs more slowly. Moreover, the temperatures at which 10 and 50% of the weight was lost, $T_{10\%}$ and $T_{50\%}$, rise up as a function of GNP volume fraction (Figure 5). The best improvement is observed for KNG-G5. It could be partially explained by the high aspect ratio and the high specific particle density (Table 2). An improvement in thermal stability by adding GNP or expanded graphite to PLA and PP has been respectively reported by Kim et al. [24], Narimissa et al. [17], and Liang et al. [40], and explained by the formation of mass transfer barriers, blocking the evaporation of the volatile degradation products. We may imagine that these barriers are more effective when the GNP are more numerous and with a greater aspect ratio, leading to a tortuous path formation. The GNP absorption on free radical produced by the thermal decomposition of PP could also improve its thermal stability [40]. To a lesser extent, the large number of KNG-150 particles compensates their low aspect ratio compared KNG-180 particles, and leads also to a significant increase of the thermal degradation temperatures. The thermal degradation temperature increase observed for

PP/KNG-G5 composites is between that of conventional PP/expanded graphene microcomposites [39] and that of PP/functionalized graphite oxide nanocomposites [26].

Figure 6 shows the complex viscosity η^* as a function of angular frequency for PP/1% GNP composites at 180°C. A Newtonian plateau is observed at low frequency for all samples (valid for all volume fractions ranging from 0.3% to 2%). The Newtonian viscosity increases as a function of volume fraction, as reported in the literature [27, 29, 30], especially for KNG-G5. Similar results were observed by Corcione et al. [16] in the case of an epoxy matrix filled with GNP of different sizes. The relative viscosity η_r, defined as the ratio of the Newtonian complex viscosity of the composite to that of the PP matrix, is plotted as a function of volume fraction in Figure 7. Data are fitted by a second order Einstein model, according to Utracki and Lyngaae-Jorgensen method in the case of platelets [41]:

$$\eta_r = 1 + [\eta]\varphi_{vol} + k([\eta]\varphi_{vol})^2 \quad (1)$$

where $[\eta]$ is the intrinsic viscosity, and k is the interaction parameter between fillers.

The aspect ratio p can be deduced from the intrinsic viscosity:

$$[\eta] = 2.5 + 0.025\,(1 + p^{1.47}) \quad (2)$$

The values of the intrinsic viscosity $[\eta]$, the interaction parameter k, and the aspect ratio p are reported in Table 3. For PP/KNG-180 and PP/KNG-150 composites, the relative viscosity η_r slightly increases as a function of volume fraction, leading to low values of interaction parameter k and aspect ratio p. These values are similar to those reported by Beuguel et al. [42] for polyamide/talc microcomposites. For PP/KNG-G5 composites, an important increase of relative viscosity is observed, of the same order of magnitude as the one obtained in the case of exfoliated organically modified montmorillonite in polyamide [42]. This is unexpected because the structure of PP/KNG-G5 composites is mainly micrometric, without exfoliation of the graphite layers. It is worth pointing out that the aspect ratio values p estimated from rheology largely overestimate those measured in TEM images (compare Table 3 and Table 2). This could be due to the use of the values proposed by Utracki and Lynngaae-Jorgensen [41] to link $[\eta]$ and p (Eq. (2)),

which were determined in the case of fully exfoliated PA/organoclay nanomposites. To elucidate this point, a Krieger-Dougherty model was also used to fit the data:

$$\eta_r = \left(1 - \frac{\varphi_{vol}}{\varphi_{max}}\right)^{-[\eta]\varphi_{max}} \quad (3)$$

where φ_{max} is the maximum volume fraction. Mueller et al. [43] proposed to link intrinsic viscosity and aspect ratio by a linear relationship:

$$[\eta] = 3.02 + 0.321\, p \quad (4)$$

The best fit of the data by Eq. (3), of the same quality as Eq. (1), provided values of p = 162 for KNG-G5 and p = 28 for KNG-150 and KNG-180, and $[\eta]$ = 55 for KNG-G5 and $[\eta]$ = 12 for KNG-150 and KNG-180. These values are very close to those obtained by the previous method and confirm that the determination of p by TEM images analysis greatly underestimates the data.

The unexpected behavior of KNG-G5 can thus be mainly explained by its high aspect ratio, even though the tactoids are not exfoliated. Indeed, p values around 200 and more were reported by Beuguel et al. [42] for exfoliated polyamide/organoclay nanocomposites. Moreover, the GNP stiffness [44] which is higher than the one of clay [45], and the filler/filler and filler/matrix interactions which are stronger between non polar components than between polar ones, because of the higher energy of London forces [46] (as suggested by the important k value (Table 3)), could amplify the relative viscosity increase, compared to polyamide/clay systems. In contrast, non-exfoliated talc/polyamide nanocomposites exhibited aspect ratio of 40, of the same order of magnitude of those of KNG-150 and KNG-180.

Figure 8 presents the variation of the storage modulus E' and loss modulus E'' as a function of temperature for PP/1% GNP composites. Mechanical properties in the linear domain, characterized by the storage E' and loss E'' moduli, are improved by the addition of GNP over the whole range of temperature as reported in the literature in the case of exfoliated graphite [30]. A more intense increase of the storage E' and loss E'' moduli is observed for the KNG-G5-based composites. This important rise is in the same order of magnitude than those measured on polyamide/organically modified montmorillonite [47] or

PP/functionalized graphene oxide nanocomposites [26]. It confirms the great reinforcement ability of the KNG-G5 graphene nanoplatelets. Because the PP crystallinity degree (as measured by DSC, results not shown in this paper) is the same in presence or not of GNP, the mechanical reinforcement seems mainly due to the intrinsic properties of GNP, as explained in the previous paragraph. However, a subsequent paper on the effect of GNP on the PP crystallization (crystal size and orientation) will confirm the main role of the intrinsic properties of GNP on the composite mechanical properties. Finally, there is no effect of the addition of GNP on the characteristic temperatures of PP relaxation in the composites, $T_\alpha \approx 5°C$ and $T_{\alpha'} \approx 70°C$, determined by tanδ peaks. An increase in tanδ above $T_{\alpha'}$ is observed for 1 and 1.5% KNG-G5 composites.

In order to quantify the effect of GNP volume fraction on mechanical properties, Figure 9 plots the storage modulus E_0' in the glassy domain ($T < T_\alpha$) as a function of GNP volume fraction. A more intense increase of the storage modulus E_0' for the KNG-G5-based composites is observed. For example, an increase of 1.1 GPa in E_0' (that is +29.4%) is measured on the composite containing 1.65% of KNG-G5 relatively to the PP matrix.

Influence of melt mixing conditions

The effect of mixing conditions on the structural and rheological properties was investigated for composites presenting the more promising properties, i.e. PP/KNG-G5.

Assuming the graphene layer dimensions to be L x l = 1 x 1 µm, the carbon interatomic distance, d_C = 0.120 nm and the graphene hexagonal mesh dimensions, L_0 = 0.208 nm and l_0 = 0.180 nm, the number of carbon atoms per layer can be estimated as $N \approx 2L/L_0\, l/l_0 \approx 53.5 \times 10^6$, corresponding to $n = N/N_A \approx 9.10^{-17}$ moles of carbon atoms, where N_A is the Avogadro number. The cohesion forces between two graphene layers are due to Van der Waals forces between carbon atoms, with a binding energy $E_0 \approx 6$ kJ.mol^{-1} [48]. The energy required to separate two graphene layers is estimated to be $E_1 = E_0 \times 2n \approx 1.1 \times 10^{-15}$ kJ.

Furthermore, the ratio between the mechanical energy dissipated during mixing and the sample weight (around 50 g) enables to deduce the specific mechanical energy SME. The mass of two graphene layers is $m = 2n \times M_C \approx 2.1 \times 10^{-15}$ g, where M_C is the carbon molar weight (M_C = 12 g.mol^{-1}). Thus, the mechanical energy applied to two graphene layers is $E_2 = SME \times m$.

Three different melt mixing conditions were applied for the dispersion phase:

- t = 6 min at a rotor speed N = 100 rpm; $SME \approx 0.4$ kJ.g^{-1}; $E_2 \approx 8.5.10^{-16}$ kJ < E_1,
- t = 6 min at a rotor speed N = 200 rpm; $SME \approx 1$ kJ.g^{-1}; $E_2 \approx 2.1.10^{-15}$ kJ > E_1,
- t = 12 min at a rotor speed N = 100 rpm; $SME \approx 0.8$ kJ.g^{-1}; $E_2 \approx 1.7.10^{-15}$ kJ > E_1.

According to these results, conditions 2 and 3 should lead to an exfoliation of the nanoplatelets, at least to a partial one. However, KNG-G5 GNP size and number appear independent of mixing conditions, as they have the same surface coverage parameter S (Table 4). Moreover, the rheological properties of PP/KNG-G5 composites are similar for all mixing conditions used (Figure 10). This result suggests that the dispersion mechanisms in such thermoplastic/compact filler composites should be more complex than only based on the mechanical energy, as proposed above.

CONCLUSION

Mechanical delamination followed by centrifugation enables to improve the performances of GNP in thermoplastics but PP/GNP composites have to be considered as non-exfoliated microcomposites. Although the GNP are not exfoliated, the thermal, rheological and mechanical properties of these composites (and especially those filled with KNG-G5) are outstandingly close to those of nanocomposites based on partially exfoliated montmorillonite or reduced graphene. This is assumed to be due to a high aspect ratio of the GNP, associated to a large rigidity of the particles. These promising properties encourage the development of this graphene manufacturing process without chemical treatment. Finally, it was shown that the investigated melt mixing conditions did not affect the structural and rheological properties of PP/GNP composites.

ACKNOWLEDGMENTS

This study was carried out in the frame of the CNRS (National Center for Scientific Research, France) research group GDR PolyNano. The GDR is acknowledged for providing the different GNP powders. The authors are grateful to their colleagues Séverine A.E. Boyer, Romain Castellani, Christelle Combeaud, Jean-Marc Haudin, Suzanne Jacomet, Gabriel Monge from MINES ParisTech – CEMEF and Sophie Pagnotta from Centre Commun de Microscopie Appliquée (CCMA), University Nice Sophia-Antipolis, for their help in their respective domains of expertise (rheometry, DMA, SEM, X-ray diffraction, TEM).

REFERENCES

[1] M. Alexandre and P. Dubois, *Mater. Sci. Eng.*, **28**, 1 (2000).

[2] E.T. Thostenson, Z. Ren and T.-W. Chou, *Compos. Sci. Technol.*, **61**, 1899 (2001).

[3] M.F.L. De Volder, S.H. Tawfick, R.H. Baughman and A.J. Hart, *Science*, **339**, 535 (2013).

[4] K.S. Novoselov, *Science*, **306**, 666 (2004).

[5] S. Stankovich, D.A. Dikin, G.H.B. Dommett, K.M. Kohlhaas, E.J. Zimney, E.A. Stach, R.D. Piner, S.T. Nguyen and R.S. Ruoff, *Nature*, **442**, 282 (2006).

[6] H. Kim, A.A. Abdala and C.W. Macosko, *Macromol.*, **43**, 6515 (2010).

[7] P. Mukhopadhyay and R.K. Gupta, *Graphite, Graphene and their Polymer Nanocomposites*, CRC Press, Taylor & Francis Group, Boca Raton (2012).

[8] S. Stankovich, D.A. Dikin, R.D. Piner, K.A. Kohlhaas, A. Kleinhammes, Y. Jia, Y. Wu, S.T. Nguyen and R.S. Ruoff, *Carbon*, **45**, 1558 (2007).

[9] H.C. Schniepp, J. Li, M.J. McAllister, H. Sai, M. Herrera-Alonso, D.H. Adamson, R.K. Prud'homme, R. Car, D.A. Saville and I.A. Aksay, *J. Phys. Chem. B*, **110**, 8535 (2006).

[10] Y. Zhu, S. Murali, M.D. Stoller, A. Velamakanni, R.D. Piner and R.S. Ruoff, *Carbon*, 48, 2118 (2010).

[11] W.S. Hummers and R.E. Offeman, *J. Am. Chem. Soc.*, **80**, 1339 (1958).

[12] G. Chen, C. Wu, W. Weng, D. Wu and W. Yan, *Polymer*, 44, 1781 (2003).

[13] A. Celzard, M. Krzesiñska, D. Bégin, J.F. Marêché, S. Puricelli and G. Furdin, *Carbon*, **40**, 557 (2002).

[14] W. Zhao, M. Fang, F. Wu, H. Wu, L. Wang and G. Chen, *J. Mater. Chem.*, **20**, 5817 (2010).

[15] J. Shen, X. Chen and W. Huang, *J. Appl. Polym. Sci.*, **88**, 1864 (2003).

[16] C. E. Corcione, F. Freuli and A. Maffezzoli, *Polym. Eng. Sci.*, **53**, 531 (2013).

[17] E. Narimissa, R.K. Gupta, N. Kao, H. J. Choi and S.N. Bhattacharya, *Polym. Eng. Sci.*, **55**, 1560 (2015).

[18] M.A. Milani, D. González, R. Quijada, N.R.S. Basso, M.L. Cerrada, D.S. Azambuja and G.B. Galland, *Compos. Sci. Technol.*, **84**, 1 (2013).

[19] S. Paszkiewicz, I. Pawelec, A. Szymczyk, Z. Spitalsky, J. Mosnacek, A. Kochmanska and Z. Roslaniec, *Polym. Eng. Sci.*, **55**, 2222 (2015).

[20] S. Chandrasekaran, C. Seidel, and K. Schulte, *Europ. Polym. J.*, **49**, 3878 (2013).

[21] H. Akhina, M.R. Gopinathan nair, N. Kalarikkai, K.P. Pramoda, T.H. Ru, L. Kalias and S. Thomas, *Polym. Eng. Sci.*, **57**, 1 (2017).

[22] J. Canales, M. Fernandez, J.J. Pena, M.E. Munoz and A. Santamaria, *Polym. Eng. Sci.*, **55**, 1142 (2015).

[23] S. Lin, M.A.S. Anwer, Y. Zhou, A. Sinha, L. Carson and H.E. Naguib, *Compos. Part B*, **132**, 61 (2018).

[24] I.H. Kim, and Y.G Jeong, *J. Polym. Sci. Part B: Polym. Phys.*, **48**, 850 (2010).

[25] P. Song, Z. Cao, Y. Cai, L. Zhao, Z. Fang and S. Fu, *Polymer*, **52**, 4001 (2011).

[26] B. Yuan, C. Bao, L. Song, N. Hong, K.M. Liew and Y. Hu, *Chem. Eng. J.*, **237**, 411 (2014).

[27] M. El Achaby, F.-E. Arrakhiz, S. Vaudreuil, A. El Kacem Qaiss, M. Bousmina and O. Fassi-Fehri, *Polym. Compos.*, **33**, 733 (2012).

[28] V. Causin, C. Marega, A. Marigo, G. Ferrara and A. Ferraro, *Eur. Polym. J.*, **42**, 3153 (2006).

[29] K. Kalaitzidou, H. Fukushima and L.T. Drzal, *Carbon*, **45**, 1446 (2007).

[30] C.I. Ferreira, O. Bianchi, M.A.S. Oviedo, R.V.B. Oliveira and R.S. Mauler, *Polímeros Ciência E Tecnol.*, **23**, 456 (2013).

[31] P.J. Hubert, K. Kathiresan and K. Wakabayashi, *Polym. Eng. Sci.*, **51**, 2273 (2011).

[32] S. He, J. Zhang, X. Xiao and X. Hong, *Polym. Eng. Sci.*, **47**, 21 (2017).

[33] T.D. Fornes, P.J. Yoon, H. Keskkula and D.R. Paul, *Polymer*, **42**, 09929 (2001).

[34] R. Zouari, T. Domenech, B. Vergnes and E. Peuvrel-Disdier, *J. Rheol.*, **56**, 725 (2012).

[35] R. Seguela, E. Staniek, B. Escaig and B. Fillon, *J. Appl. Polym. Sci.*, **71**, 1873 (1999).

[36] Y. Li, Q.. Fang, Z. Yi and K. Zheng, *Mater. Sci. Eng. A.*, **370**, 268 (2004).

[37] C.I. Ferreira, C. Dal Castel, M.A.S. Oviedo and R.S. Mauler, *Thermochim. Acta.*, **553**, 40 (2013).

[38] S.G. Prolongo, A. Jimenez-Suarez, R. Moriche and A. Urena, *Europ. Polym. J.*, **53**, 292 (2014).

[39] E.E. Kiziltas, A.J. Duguay, A. Kiziltas, B. Nazari, J.W. Nader, D.J. Gardner and T.S. Rushing, *Polym. Compos.*, DOI 10.1002/pc.24400 (2017).

[40] J.Z. Liang, J.Z. Wang, G.C.P. Tsui and C.Y. Tang, *J. Thermoplast. Compos. Mater.*, **48**, 1 (2017).

[41] L.A. Utracki and J. Lyngaae-Jørgensen, *Rheol. Acta.*, **41**, 394 (2202).

[42] Q. Beuguel, J. Ville, J. Crepin-Leblond, P. Mederic and T. Aubry, *Polymer*, **62**, 109 (2015).

[43] S. Mueller, E.W. Llewellin and H.M. Mader, *Proc. Royal Soc. A*, **466**, 1201 (2010).

[44] C. Lee, X. Wei, J.W. Kysar and J. Hone, *Science*, **321**, 385 (2008).

[45] D. Ebrahimi, R.J.-M. Pellenq and A.J. Whittle, *Langmuir*, **28**, 16855 (2012).

[46] J.N. Israelachvili, *Van der Waals Forces*, in: Intergovernmental Panel on Climate Change (Ed.), Intermol. Surf. Forces, Elsevier, Cambridge, 107–132 (2011).

[47] T. Liu, K. Ping Lim, W. Chauhari Tjiu, K.P. Pramoda and Z.-K. Chen, *Polymer*, **44**, 3529 (2003).

[48] Y. Si and E.T. Samulski, *Nano Lett.*, **8**, 1679 (2008).

TABLE CAPTIONS:

TABLE 1 Bulk density, density, carbon content, particle diameter *d*, thickness *e*, and specific area of the used GNP (supplier data)

TABLE 2 Actual volume fraction ϕ_{vol}, surface coverage S, average lateral dimension L, thickness e, aspect ratio p_{MET} and specific particle density d_{sp} of GNP into the composites at a volume fraction of around 1%

TABLE 3 Intrinsic viscosity [η], interaction parameter *k*, and aspect ratio *p* of GNP in the composites

TABLE 4 Surface coverage *S* of KNG-G5 microparticles in the composites for various mixing conditions and two GNP volume fractions

FIGURE CAPTIONS :

Figure 1 SEM images of KNG-180 (a), KNG-150 (b) and KNG-G5 (c) powders

Figure 2 SEM (a-c) and TEM (d-f) images of PP/KNG-180 (a, d); PP/KNG-150 (b, e) and PP/KNG-G5 (c, f) composites with 1% GNP volume fraction

Figure 3 Wide angle X-Ray diffractograms of PP/GNP composites. The inset is a zoom on the peak characterizing the graphene stack (002). — PP, --- 1% KNG-180, –––0.9% KNG-150, -•-•- 1.05% KNG-G5

Figure 4 Thermogravimetric analyses of PP/GNP composites. Mass variation with temperature

Figure 5 Thermal degradation temperatures, (a) $T_{10\%}$ and (b) $T_{50\%}$, of PP/GNP composites as a function of GNP volume fraction. The lines are just to guide the eyes.

Figure 6 Complex viscosity η^* at 180°C as a function of angular frequency for PP/GNP composites: □ PP, ● 1% KNG-180, ○ 0.9% KNG-150, ■ 1.05% KNG-G5

Figure 7 Relative viscosity η_r of PP/GNP composites at 180°C as a function of GNP volume fraction. Symbols are experimental points and the full lines correspond to the Einstein model fits (Eq. (1))

Figure 8 Storage, E', and loss, E'', moduli as a function of temperature for PP/GNP composites: □ PP, ● 1% KNG-180, ○ 0.9% KNG-150, ■ 1.05% KNG-G5

Figure 9 Storage modulus in the glassy domain, E_0', of PP/GNP composites as a function of GNP volume fraction. The lines are just to guide the eyes.

Figure 10 Complex viscosity η^* as a function of angular frequency of PP/KNG-G5 composites prepared in various mixing conditions: ○ 6 min, 100 rpm, □ 6 min, 200 rpm, △ 12 min, 100 rpm

TABLE 1 Bulk density, density, carbon content, particle diameter *d*, thickness *e*, and specific area of the used GNP (supplier data)

Sample	Bulk density (-)	Density (-)	Carbon content (%wt)	*d* (µm)	*e* (nm)	Specific area (m^2/g)
KNG-180	0.15	2.25	> 99.5	8-100	< 100	35
KNG-150	0.20	2.25	> 98	1-20	< 15	30-60
KNG-G5	0.10	2.25	> 99	0.1-5	< 5	–

TABLE 2 Actual volume fraction ϕ_{vol}, surface coverage *S*, average lateral dimension *L*, thickness *e*, aspect ratio p_{MET} and specific particle density d_{sp} of GNP into the composites at a volume fraction of around 1%

Sample	ϕ_{vol} (%)	*S* (%)	*L* (μm)	*e* (μm)	p_{MET} (-)	d_{sp} (part./ μm^2)
PP/KNG-180	1.0	1.0	2.9	0.4	8	0.01
PP/KNG-150	0.9	0.9	1.0	0.2	5	0.03
PP/KNG-G5	1.05	0.2	1.2	0.1	10	0.04

TABLE 3 Intrinsic viscosity [η], interaction parameter k, and aspect ratio p of GNP in the composites

Sample	[η] (-)	k (-)	p (-)
PP/KNG-180	16	0.2	70
PP/KNG-150	16	0.2	70
PP/KNG-G5	50	1.8	170

TABLE 4 Surface coverage *S* of KNG-G5 microparticles in the composites for various mixing conditions and two GNP volume fractions

Sample	Mixing conditions	ϕ_{vol} (%)	*S* (%)
PP/KNG-G5	100 rpm, 6 min	1.05	0.2
PP/KNG-G5	200 rpm, 6 min	1	0.2
PP/KNG-G5	100 rpm, 12 min	1.05	0.2
PP/KNG-G5	100 rpm, 6 min	1.6	0.3
PP/KNG-G5	200 rpm, 6 min	1.65	0.3
PP/KNG-G5	100 rpm, 12 min	1.65	0.3

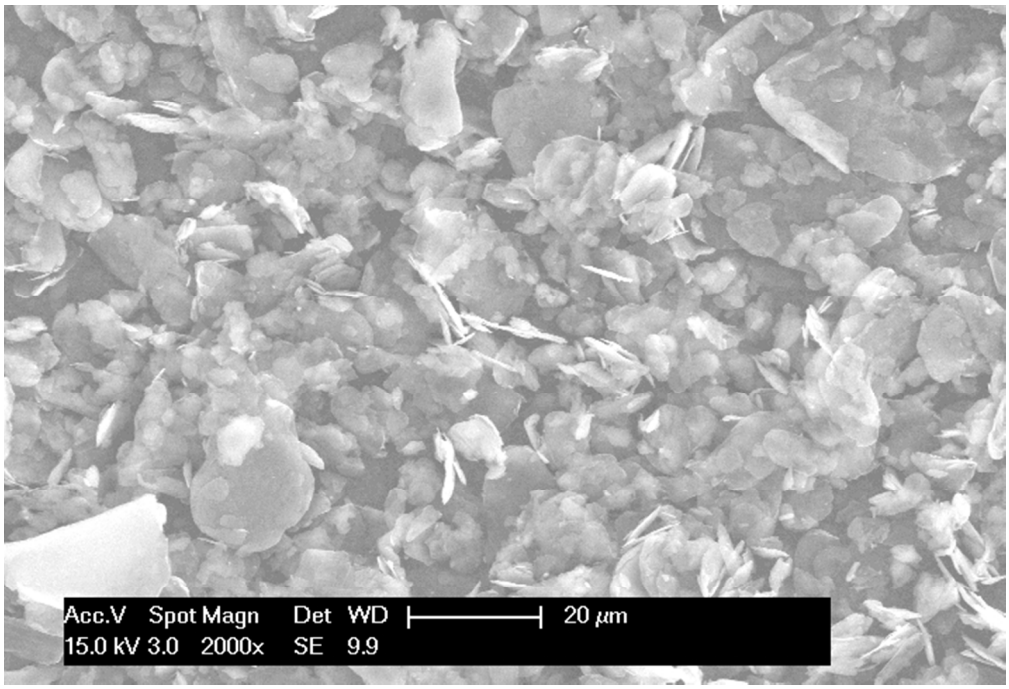

Figure 1a: SEM micrographs of KNG-180 powders

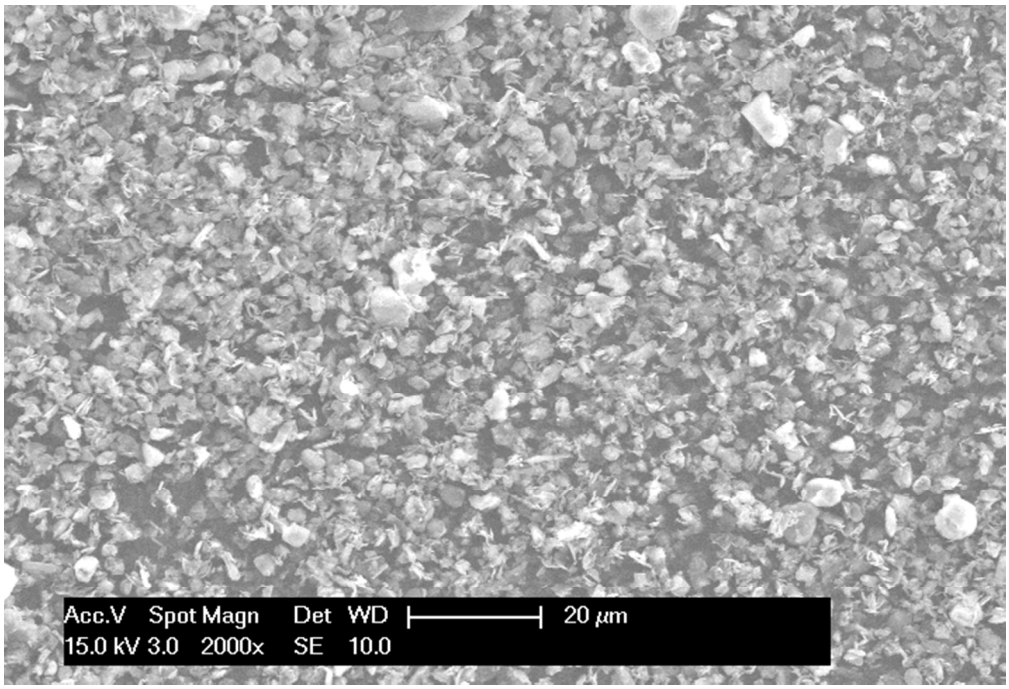

Figure 1b: SEM micrographs of KNG-150 powders

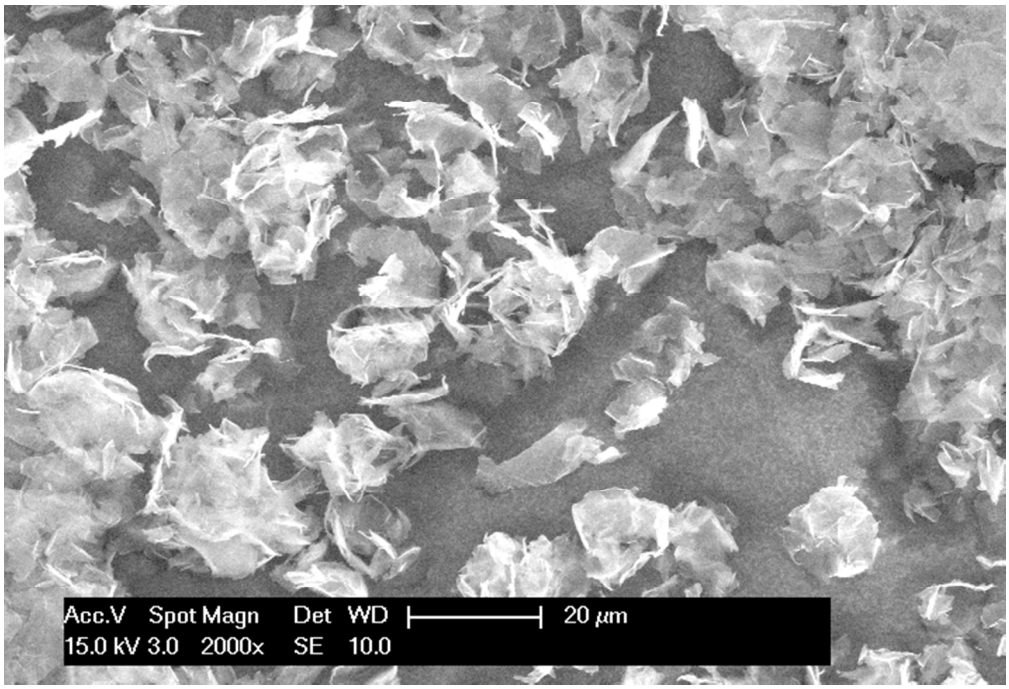

Figure 1c: SEM micrographs of KNG-G5 powders

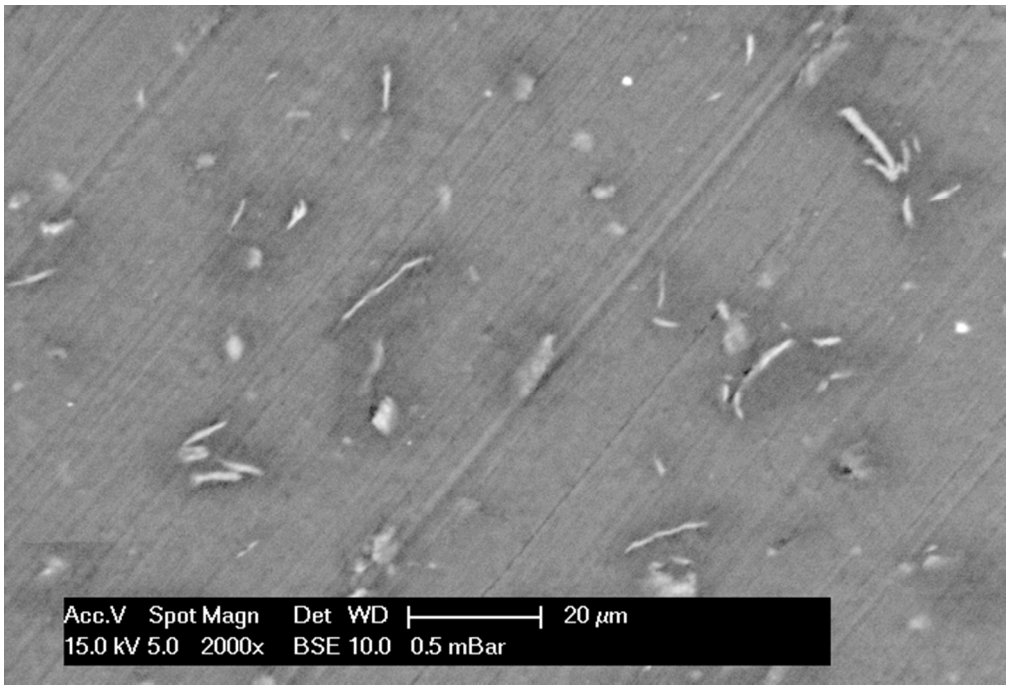

Figure 2a: SEM micrograph of PP/KNG-180 composite with 1% GNP volume fraction

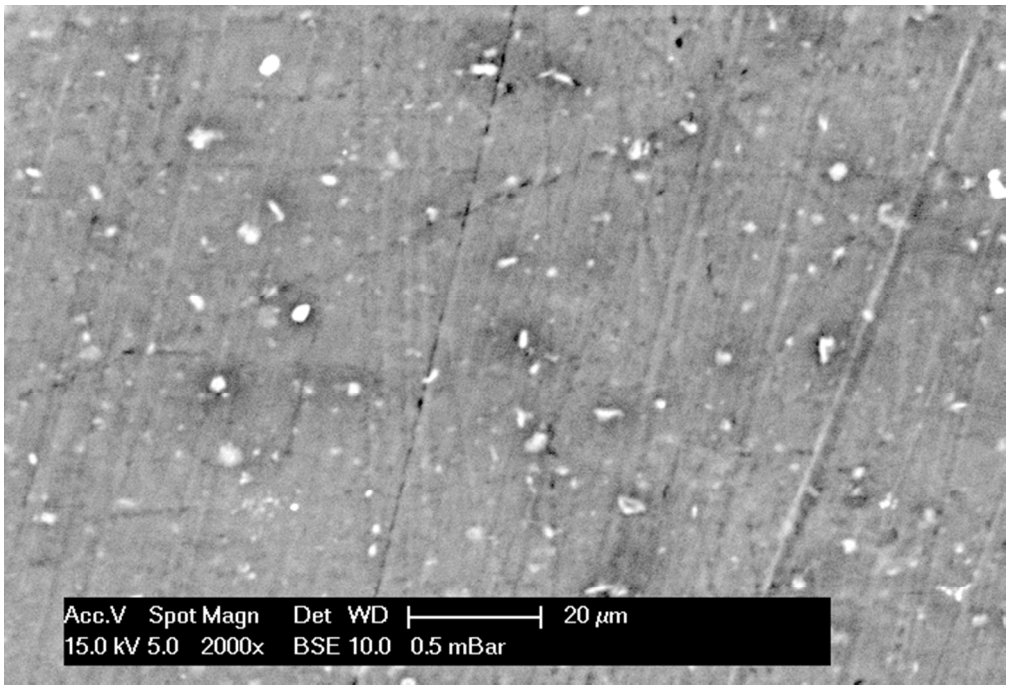

Figure 2b: SEM micrograph of PP/KNG-150 composite with 1% GNP volume fraction

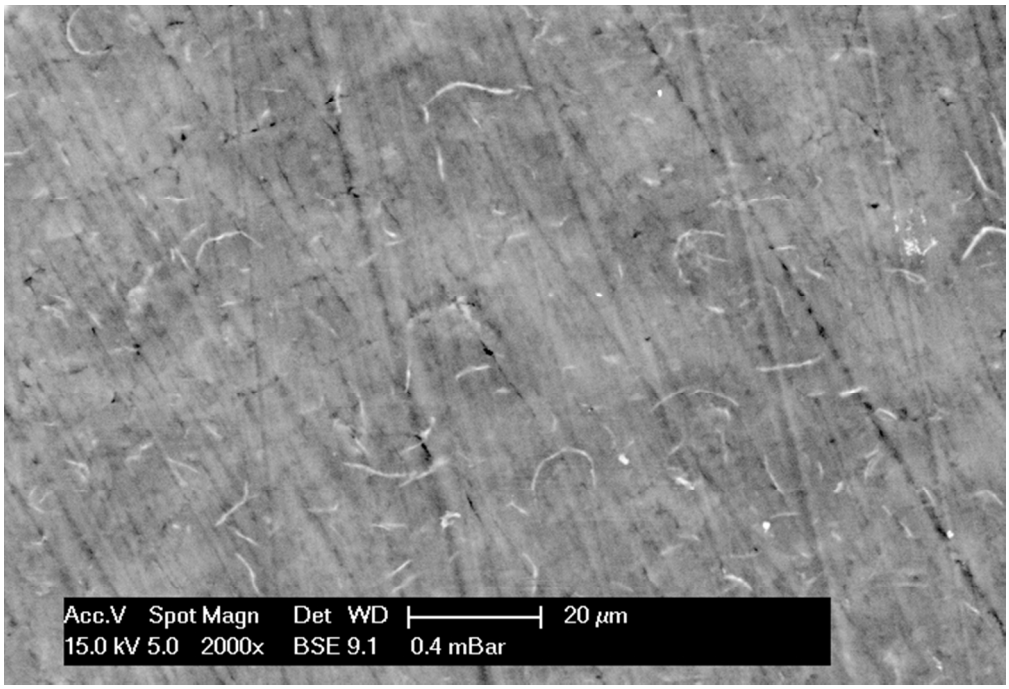

Figure 2c: SEM image of PP/KNG-G5 composite with 1% GNP volume fraction

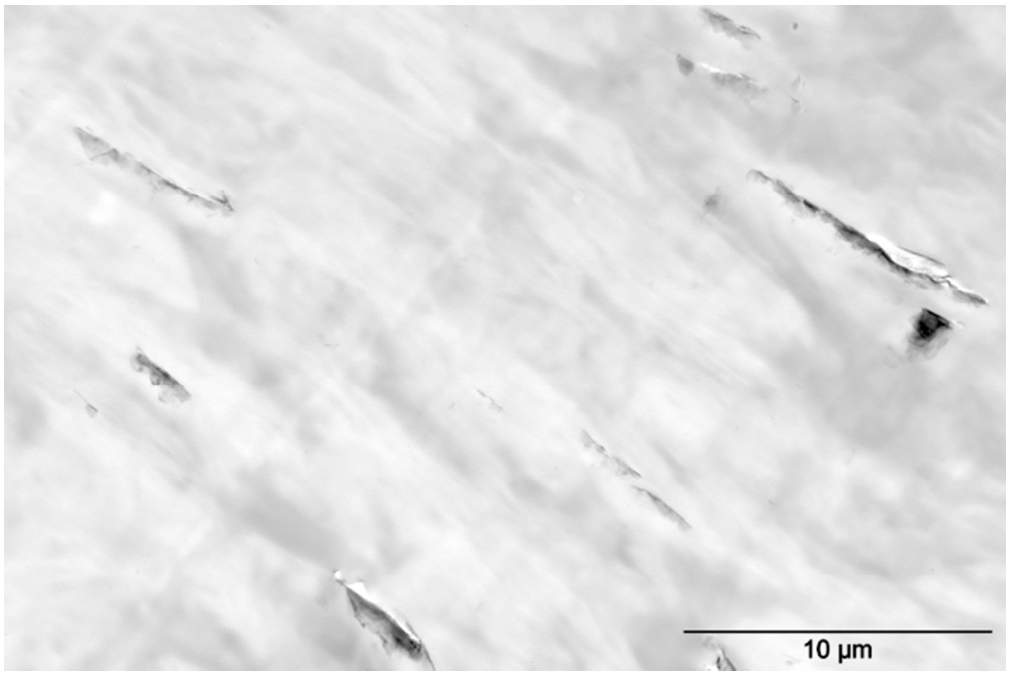

Figure 2d: TEM image of PP/KNG 180 composite with 1% GNP volume fraction

60x40mm (300 x 300 DPI)

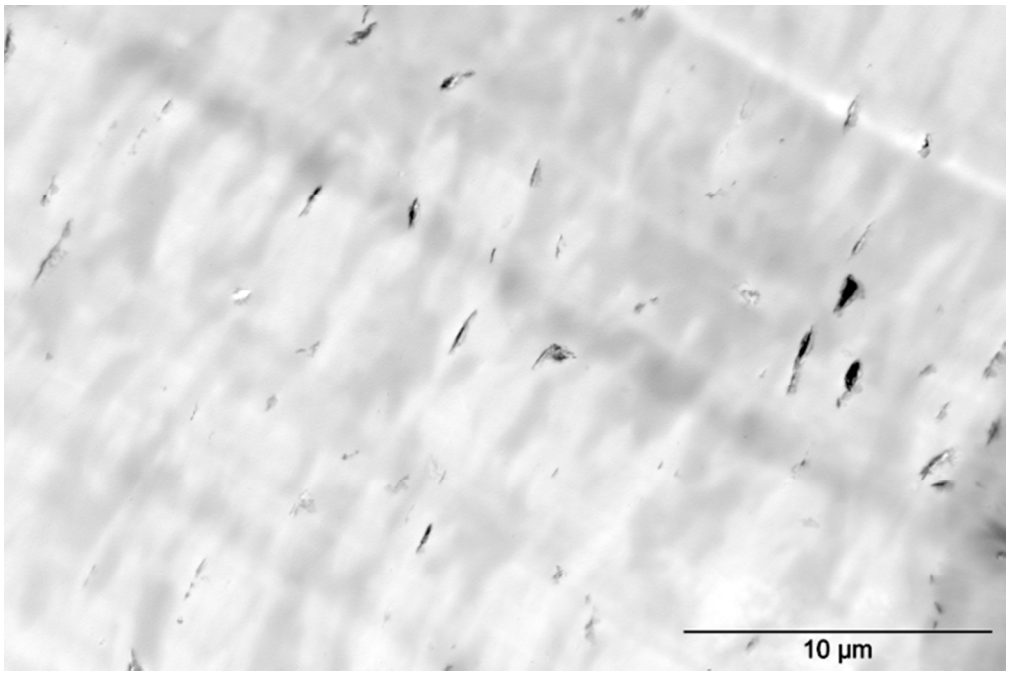

Figure 2e: TEM image of PP/KNG 150 composite with 1% GNP volume fraction

60x40mm (300 x 300 DPI)

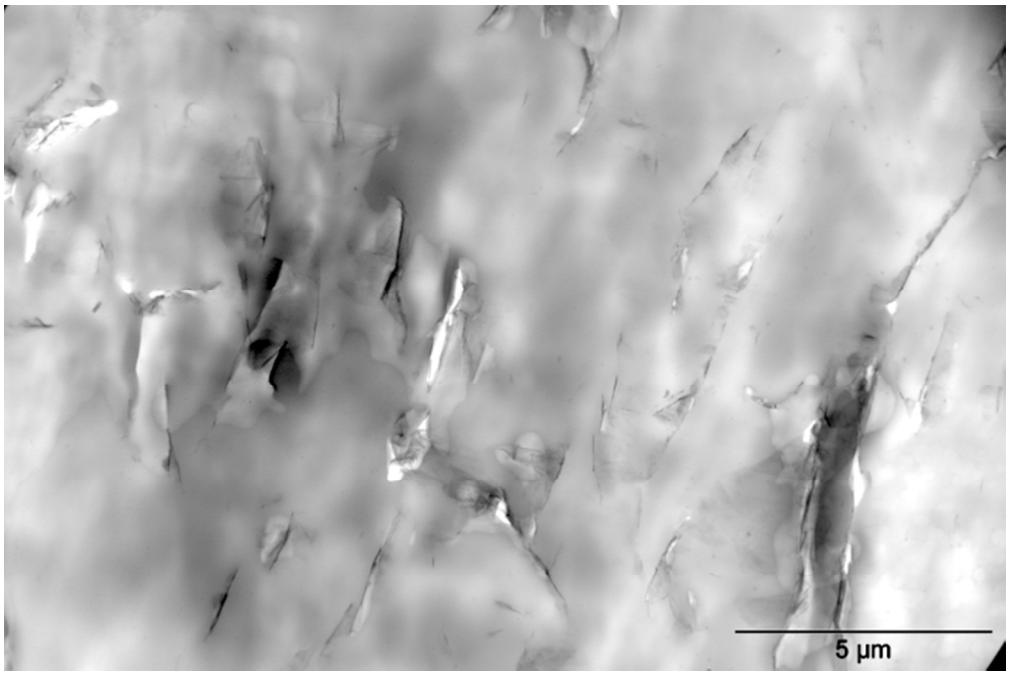

Figure 2f: TEM image of PP/KNG-G5 composite with 1% GNP volume fraction

60x40mm (300 x 300 DPI)

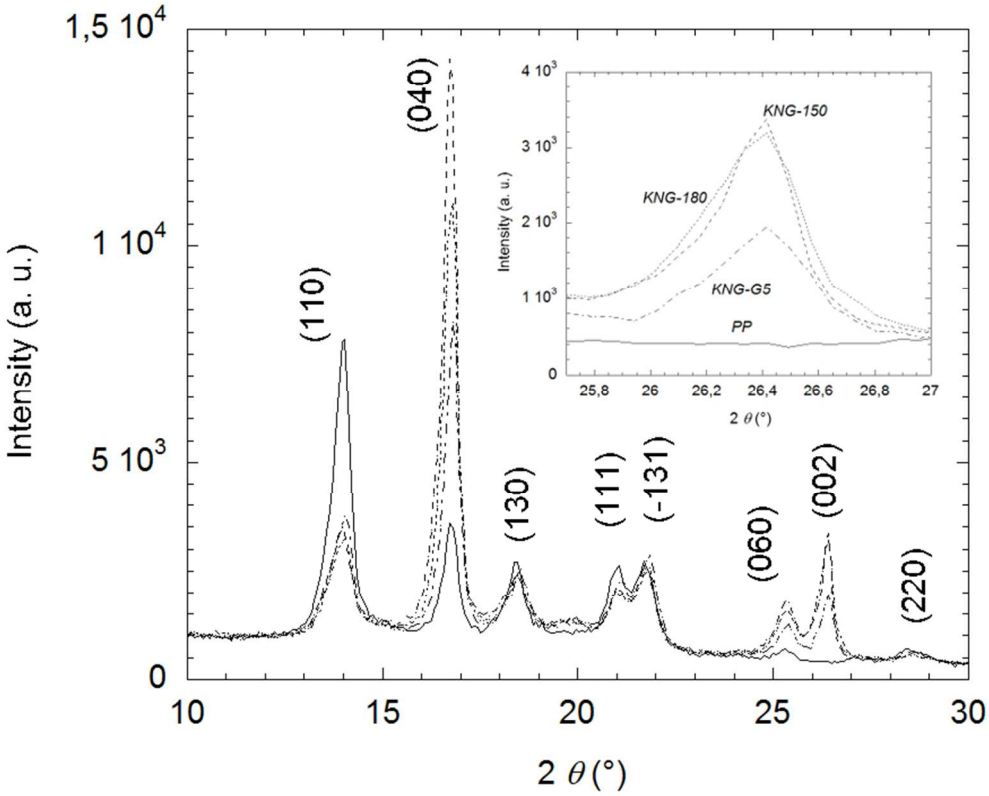

Figure 3: Wide angle X-Ray diffractograms of PP/GNP composites. The inset is a zoom on the peak characterizing the graphene stack (002). ── PP, --- 1% KNG-180, –––0.9% KNG-150, -•-•- 1.05% KNG-G5

78x63mm (288 x 288 DPI)

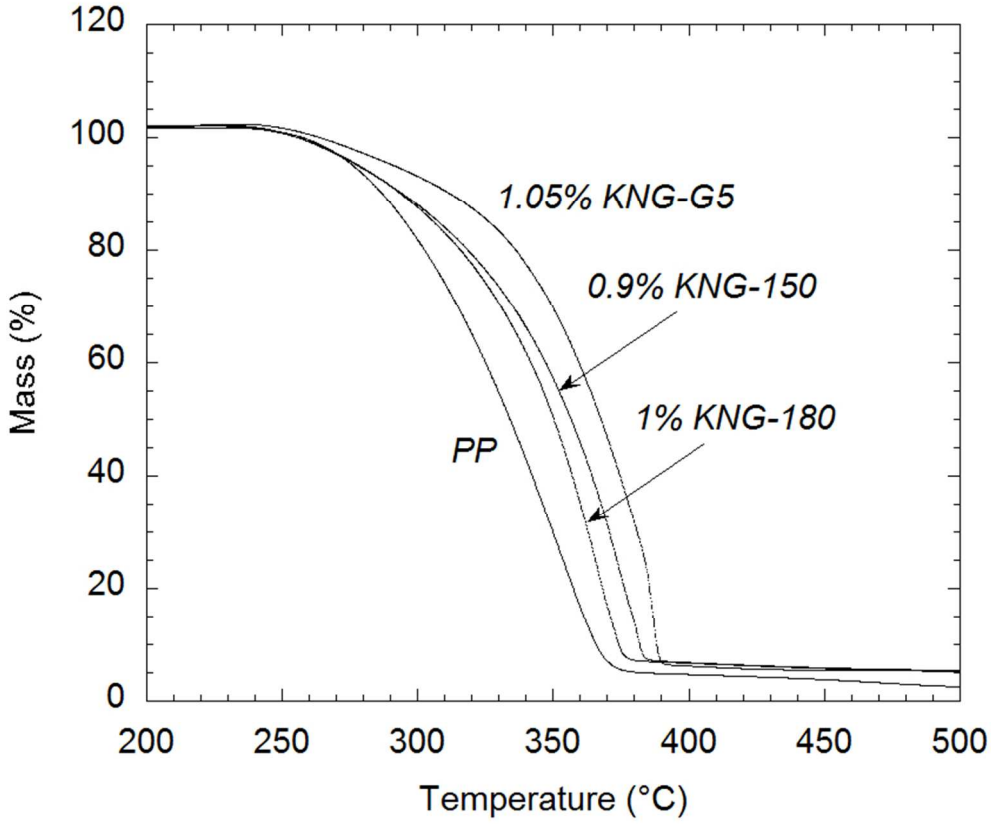

Figure 4: Thermogravimetric analyses of PP/GNP composites. Mass variation with temperature

75x62mm (288 x 288 DPI)

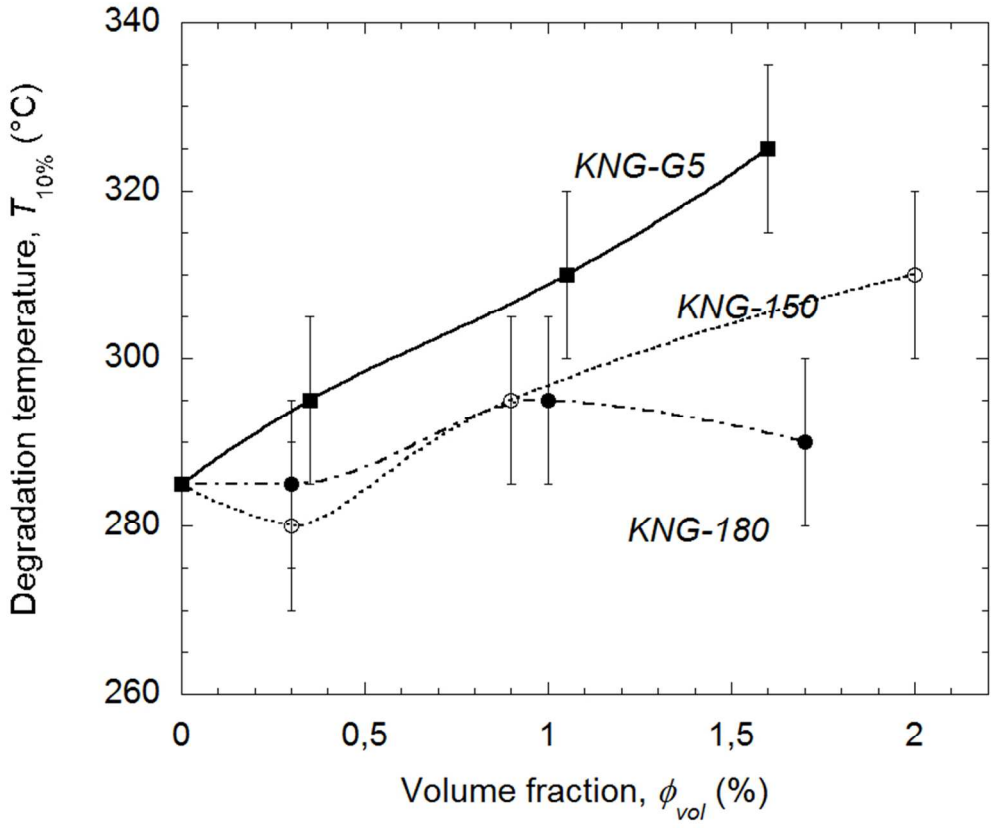

Figure 5a: Thermal degradation temperatures, (a) $T_{10\%}$, of PP/GNP composites as a function of GNP volume fraction. The lines are just to guide the eyes.

75x64mm (288 x 288 DPI)

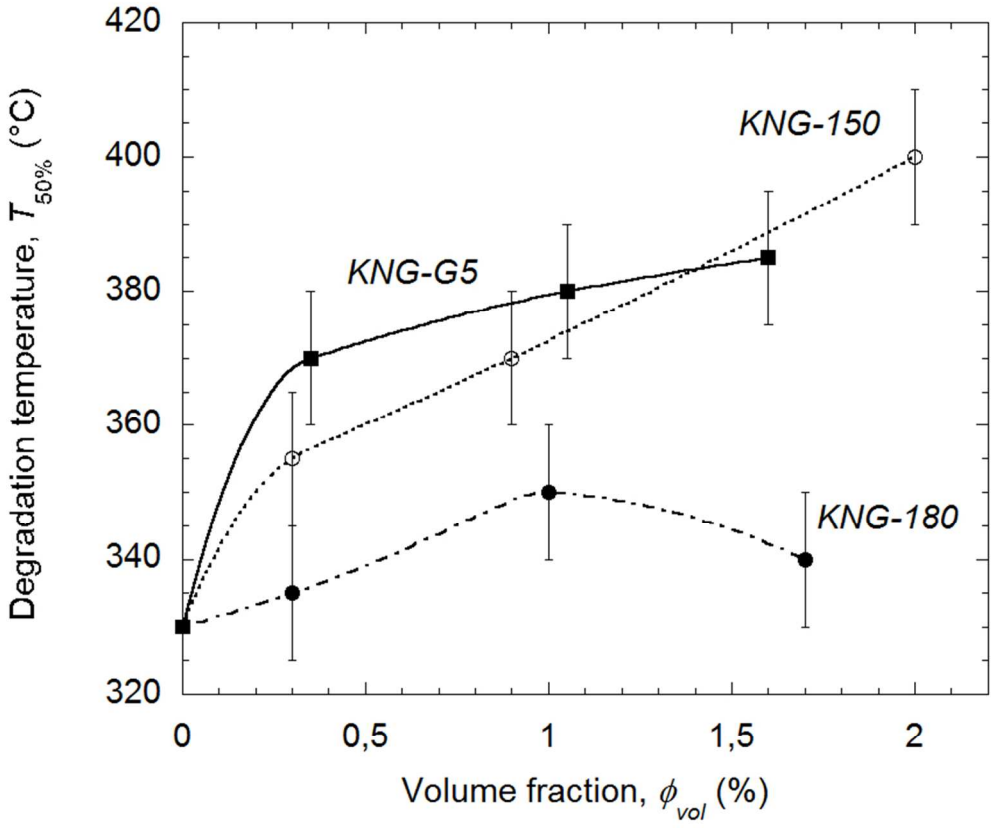

Figure 5b: Thermal degradation temperatures, (b) $T_{50\%}$, of PP/GNP composites as a function of GNP volume fraction. The lines are just to guide the eyes.

75x64mm (288 x 288 DPI)

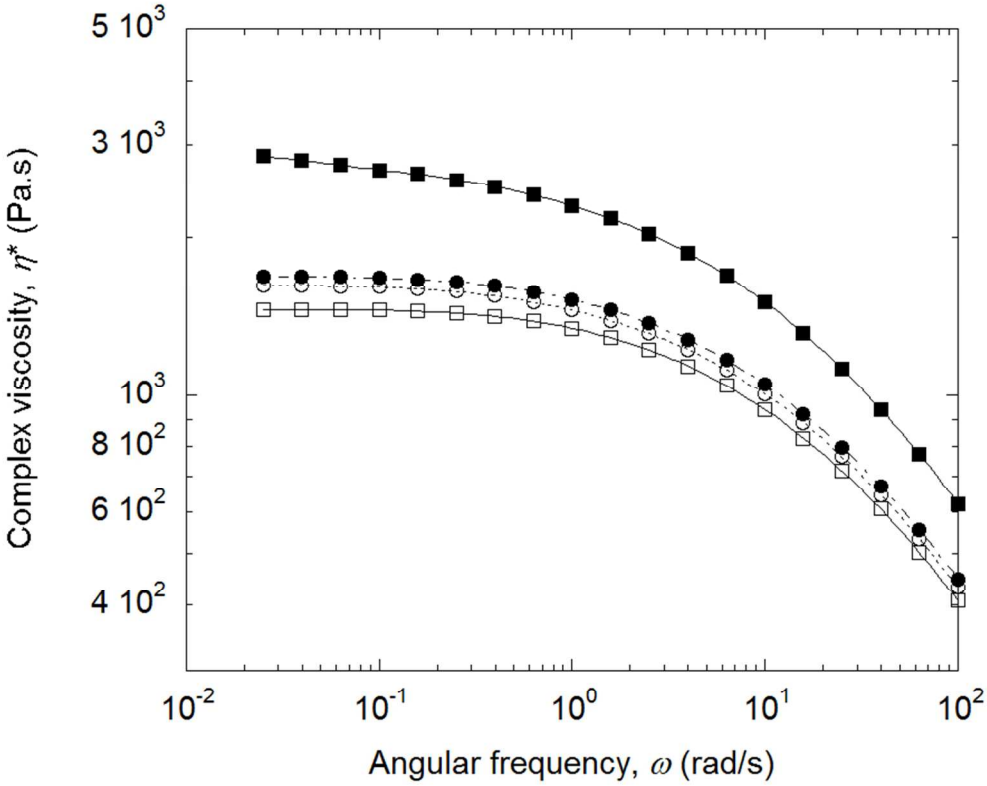

Figure 6: Complex viscosity η* at 180°C as a function of angular frequency for PP/GNP composites: □ PP, ● 1% KNG-180, ○ 0.9% KNG-150, ■ 1.05% KNG-G5

79x64mm (288 x 288 DPI)

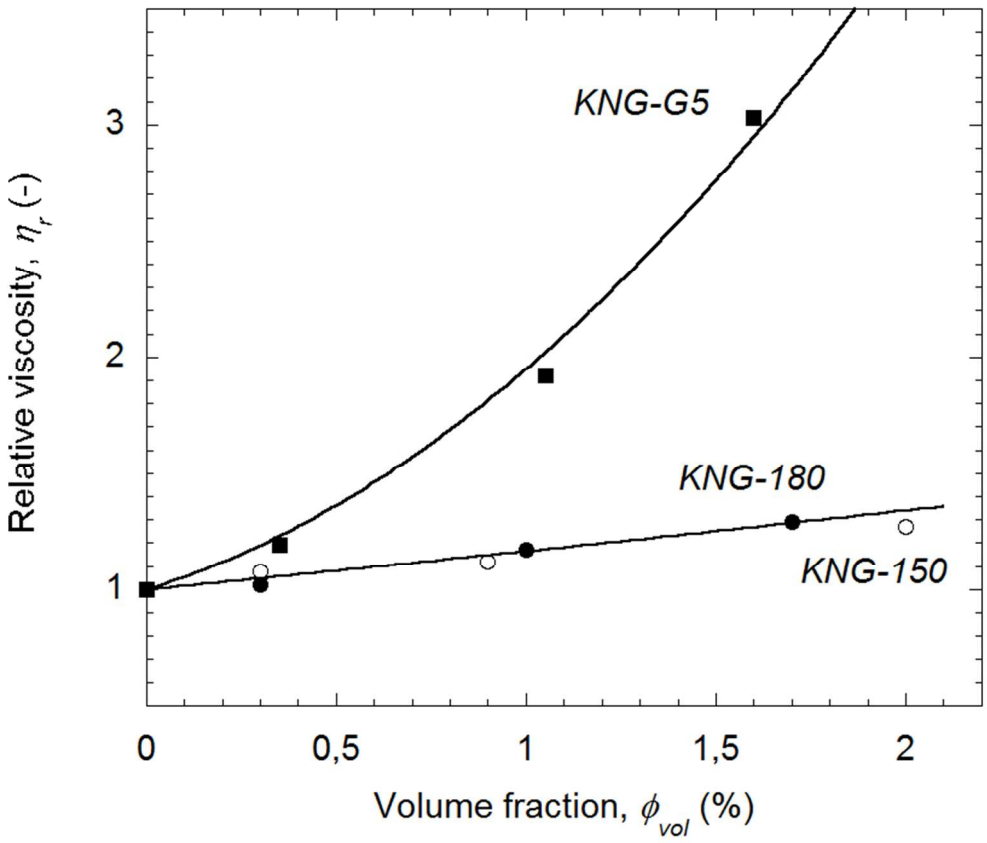

Figure 7: Relative viscosity η_r of PP/GNP composites at 180°C as a function of GNP volume fraction. Symbols are experimental points and the full lines correspond to the Einstein model fits (Eq. (1))

72x64mm (288 x 288 DPI)

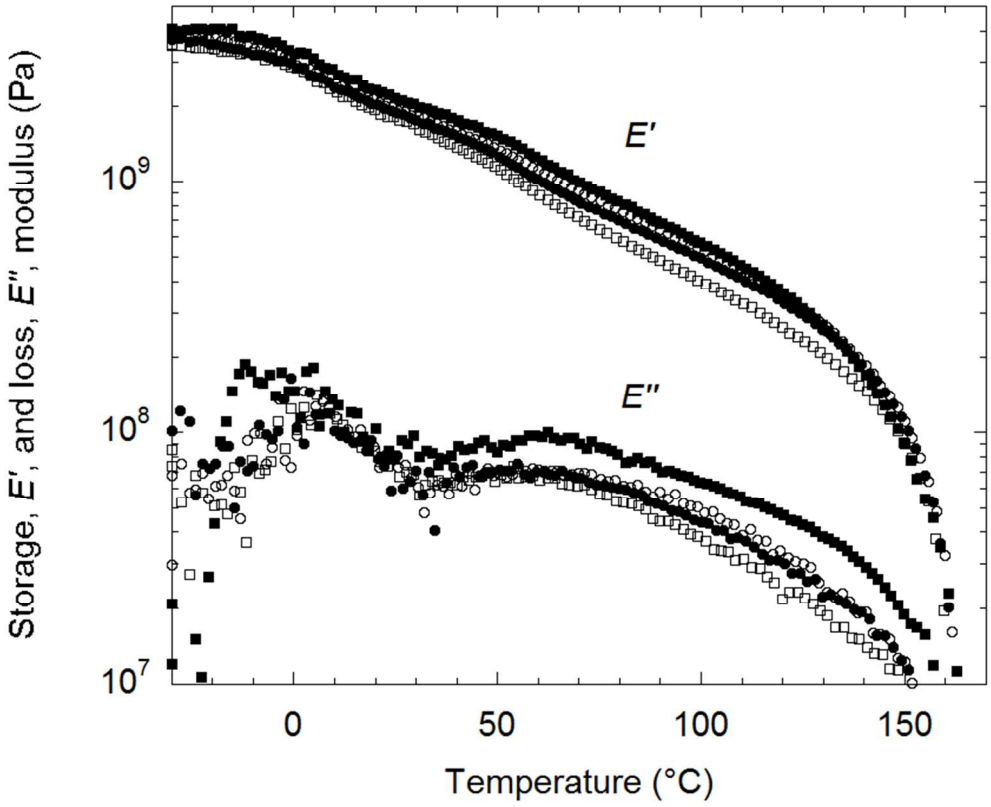

Figure 8: Storage, E', and loss, E'', moduli as a function of temperature for PP/GNP composites: □ PP, ● 1% KNG-180, ○ 0.9% KNG-150, ■ 1.05% KNG-G5

74x62mm (288 x 288 DPI)

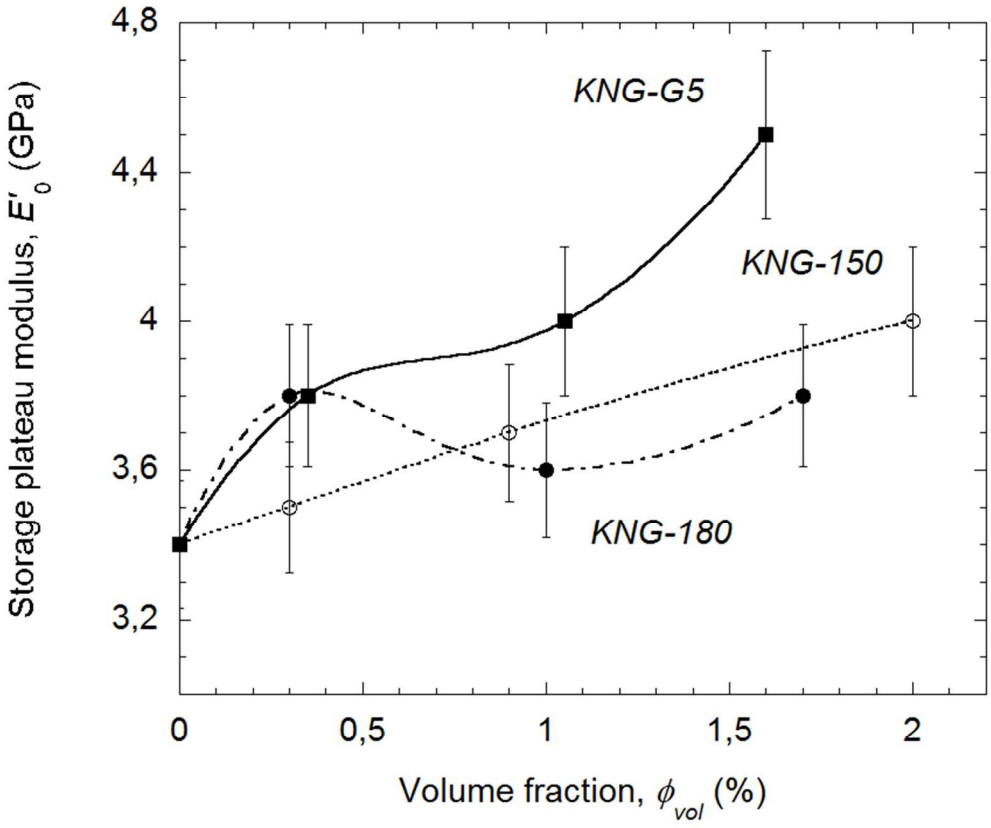

Figure 9: Storage modulus in the glassy domain, E_0', of PP/GNP composites as a function of GNP volume fraction. The lines are just to guide the eyes.

75x64mm (288 x 288 DPI)

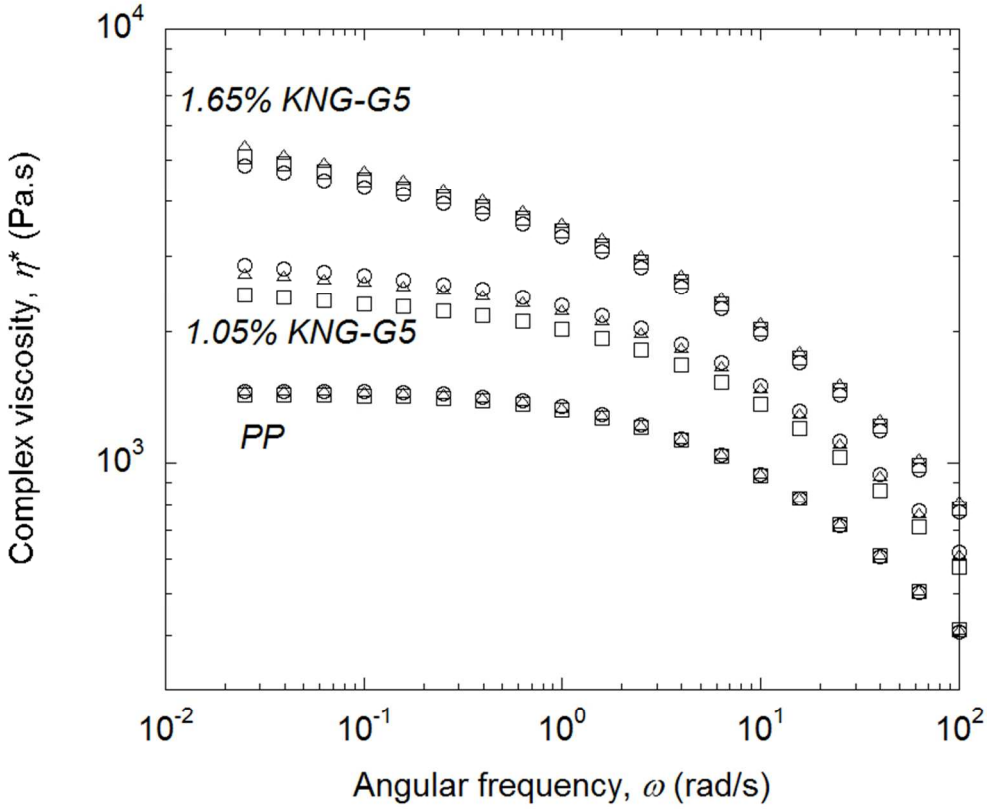

Figure 10: Complex viscosity η* as a function of angular frequency of PP/KNG-G5 composites prepared in various mixing conditions: ○ 6 min, 100 rpm, □ 6 min, 200 rpm, Δ 12 min, 100 rpm

76x64mm (288 x 288 DPI)